Observation of Photoconductivity in Sn-Doped ZnO Nanowires and Their Photoenhanced Field Emission Behavior

ARTICLE *in* THE JOURNAL OF PHYSICAL CHEMISTRY C · FEBRUARY 2010

Impact Factor: 4.77 · DOI: 10.1021/jp911080f

6 AUTHORS, INCLUDING:

Farid Jamali Sheini
Islamic Azad University, Ahwaz branch, Ah…
64 PUBLICATIONS **499** CITATIONS
SEE PROFILE

Mahendra More
Savirtibai Phule Pune University
185 PUBLICATIONS **1,659** CITATIONS
SEE PROFILE

Sandesh Jadkar
Savirtibai Phule Pune University
96 PUBLICATIONS **534** CITATIONS
SEE PROFILE

Observation of Photoconductivity in Sn-Doped ZnO Nanowires and Their Photoenhanced Field Emission Behavior

Farid Jamali Sheini,[†,‡] Mahendra A. More,[§] Sandesh R. Jadkar,[§] K. R. Patil,[⊥] Vijaymohanan K. Pillai,[⊥] and Dilip S. Joag*[,§]

Islamic Azad University, Ahwaz Branch, Ahwaz, Iran, Center for Advanced Studies in Materials Science and Condensed Matter Physics, Department of Physics, University of Pune, Pune 411007, India, and Physical and Materials Chemistry Division, National Chemical Laboratory, Pune 411008, India

Received: November 17, 2009; Revised Manuscript Received: January 11, 2010

Sn-doped ZnO nanowire films have been successfully synthesized by electrodeposition on zinc foil followed by annealing in air at 400 °C for 4 h. The XRD patterns of the annealed specimens exhibit a set of well-defined diffraction peaks indexed to the wurtzite phase of ZnO. The surface morphology of the as-synthesized films showed a network of densely packed flakes/sheets on the substrate. However, upon annealing, the formation of ZnO nanowires, processing length in the range of several micrometers and diameter less than 150 nm, on the entire substrate is observed. The relative atomic percentage of Sn, estimated from the energy dispersive spectra, was found to be 0.5 and 2.0 in the ZnO films deposited for 10 and 40 min durations, respectively. From the field emission studies, the values of the turn-on field and threshold field, required to draw emission current density of 10 and 100 μA/cm^2, are observed to be 0.68 and 1.1 V/μm for 0.5% Sn-doped ZnO and 1.72 and 2.25 V/μm for 2.0% Sn-doped ZnO, respectively. The field emission current stability investigated for a duration of 6 h at the preset value of 100 μA is found to be excellent. A prominent photoenhancement in the field emission current upon visible light illumination of the Sn-doped ZnO nanowires films has been observed. This enhancement has been attributed to the photoconductivity of the Sn-doped ZnO.

Introduction

Zinc oxide (ZnO) is an important multifunctional II−IV semiconductor with a set of unique properties suitable for a wide range of emerging applications such as optoelectronics, nanoelectronic, and spintronics devices.[1] Consequently, many low dimensional ZnO structures have been reported in the past few years, such as nanoparticles,[2] wires,[3] tubes,[4] marigolds/multipods,[5] belts,[6] rings,[7] helixes/springs,[8] and combs,[9] enabling unique size and shape dependent properties. For example, mobility of carriers in a nanowire is reported to be 100 times more than that in a spherical particle.[10] Various methods including pulsed laser deposition,[11] chemical vapor deposition,[12] catalysis-driven molecular beam epitaxy,[13] thermal evaporation,[5] and electrochemical deposition[14,15] have been employed to synthesize these ZnO nanostructures with high selectivity and yield both in powder and in thin film forms. Most of these growth processes are controlled by a fine balance between the electrostatic energy contributed by the Zn^{2+} and O^{2-} ions and the elastic deformation energy so that different metastables shapes are formed corresponding to the minimum energy configuration.[16]

As is well-known, doping of semiconductors with selective elements offers an effective approach to tailor the electrical, optical, and magnetic properties. For instance, it has been amply demonstrated that ZnO could be doped with the group III (Al, In, Ga) and group IV (Sn, Pb) elements for obtaining the desired level of electrical/optical properties.[17–22] For widespread applications of ZnO nanostructures in nanoscale electronic and photonic devices, it is necessary to find a suitable route to dope the ZnO nanostructures. Recently, we have reported the field emission behavior of undoped and doped metal oxides such as ZnO and SnO_2 prepared using electrodeposition and thermal evaporation routes.[23,24] Nevertheless, synthesis of mixed oxide nanostructures of ZnO and SnO_2 by electrodeposition route and formation of Sn-doped ZnO nanostructutres by annealing the same has not been yet attempted.

In this paper, we report the field emission characteristics of Sn-doped ZnO nanowires synthesized by cathodic electrodeposition on the zinc substrate. We also report some novel observations on photoenhanced field emission from these nanowires under the illumination of visible light. The values of the turn-on field required to draw emission current density of 10 μA/cm^2 from 0.5% and 2.0% Sn-doped ZnO nanowires, 0.68 and 1.72 V/μm, respectively, are seen to be significantly lower than those reported previously.[23,25–27] More interestingly, these Sn-doped ZnO nanowire emitters exhibit excellent emission current stability at a preset value of ∼100 μA over a duration of 6 h along with a pronounced optical switching effect at different time intervals. The enhancement in the field emission current upon illumination has been attributed to the photoconductivity of Sn-doped ZnO.

Experimental Methods

Synthesis of all the Sn-doped ZnO nanostructures in thin film form was performed in a conventional three electrode cell in aqueous solution containing a mixture of $ZnCl_2$, $SnCl_2$, and H_2O_2 (analytical grade) as a supporting electrolyte. The concentrations

* Corresponding author. E-mail: dsj@physics.unipune.ernet.in.
[†] Islamic Azad University.
[‡] Present address: Dept. of Physics, University of Prune.
[§] University of Pune.
[⊥] National Chemical Laboratory.

10.1021/jp911080f
Published on Web 02/17/2010

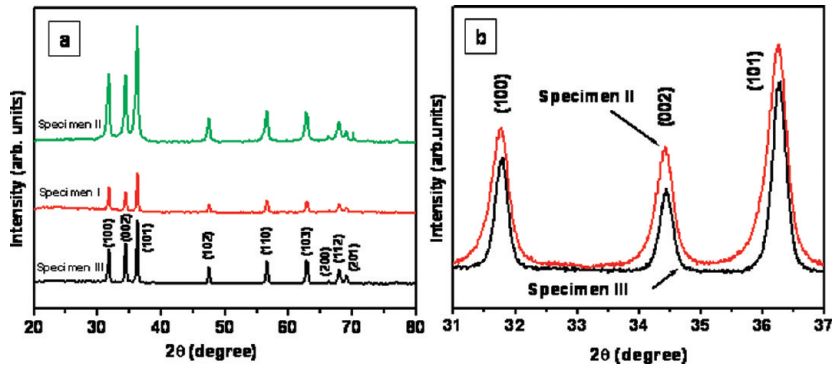

Figure 1. XRD patterns of (a) specimen I, II, and III postannealed in air at 400 °C recorded in the 2θ range of 20°−80°; (b) specimen II and III (postannealed) obtained at low scan rate in the 2θ range of 31°−37°.

of $ZnCl_2$, $SnCl_2$, and H_2O_2 in the electrolyte were kept constant at 16×10^{-3}, 16×10^{-3}, and 4×10^{-3} M, respectively. All the deposition experiments were carried out at 80 ± 2 °C, in which a polycrystalline Zn foil (purity ∼ 99.99%, Alfa Aesar), a platinum sheet, and a saturated calomel electrode (SCE, E_0 = 0.244 V) were used as the working, counter, and reference electrodes, respectively. Prior to each electrodeposition experiment, the Zn foil and the platinum electrode were ultrasonically cleaned in acetone and methanol for 10 min in each solvent, respectively. A computer-controlled electrochemical analyzer (Model-1100A Series, CH Instrument, U.S.) was used to maintain the cathodic polarization condition at −1.4 V with respect to the SCE. In order to obtain different concentration of Sn as dopant, depositions were carried out at different time intervals of 10 and 40 min, the specimens named as I and II, respectively. In order to get uniform mass transfer conditions, the electrolyte was constantly stirred during the synthesis. For a comparative study, ZnO thin films were also prepared under identical experimental conditions without adding $SnCl_2$ into the electrolyte for 40 min deposition time, the specimen named as III. The Zn foil (substrate), after the fixed deposition time, was removed from the electrolyte, immersed in distilled water, and dried in air. For each case, the "as-synthesized" thin films were annealed in air at ∼400 °C for 4 h.

At least four specimens were synthesized under identical experimental conditions and characterized by various analytical techniques in order to check the reproducibility and repeatability of the results.

The specimens were characterized by X-ray diffractometer (Model-D8, Advance, Bruker AXS) and scanning electron microscopy (SEM, JEOL, JSM-6360A). The elemental composition was obtained using an energy-dispersive X-ray spectrometer (EDS) attached to the SEM. The optical properties were investigated from the photoluminescence (PL) spectra recorded at room temperature using a xenon lamp as the source (Photoluminescence Spectrometer, Perkin-Elmer-LS-55). The excitation wavelength used was ∼325 nm. The chemical analysis of the ZnO films was performed using X-ray photoelectron spectroscopy (XPS, VG Microtech ESCA 3000). The XPS spectra were recorded at the base pressure of 10^{-10} mbar using Mg Kα radiation (1253.6 eV, line width 0.7 eV) generated at a power of 150 W. The field emission current versus applied voltage ($I-V$) and current versus time ($I-t$) characteristics were measured in a planar diode configuration in a vacuum chamber evacuated to a base pressure of $\sim 1.0 \times 10^{-8}$ mbar. The specimen served as a cathode, and a semitransparent phosphor screen, used as an anode, was held parallel to the cathode at a distance of ∼ 1 mm. The details of the field emission system and vacuum processing of the chamber are explained elsewhere.[5] The emission current was acquired by varying the applied dc voltage between the cathode and anode with a step of 40 V (0−40 kV, Spellman, U.S.). Special care was taken to avoid any leakage current by ensuring proper grounding. At least two specimens, synthesized under identical experimental conditions, were studied to check the reproducibility of the field emission results. Photoenhanced field emission was observed by illuminating the specimen with visible light (halogen lamp, 1300 W). The cathode was illuminated from the "front side" by keeping the halogen lamp at a distance of 10 cm from the view port of the chamber. The intensity of incident light at the cathode site was calibrated using a photocell and was found to be ∼80 W at the surface of the specimen.

Results and Discussions

Synthesis of all the Sn-doped ZnO nanostructures in thin film form was performed in a conventional three electrode cell in aqueous solution containing a mixture of $ZnCl_2$, $SnCl_2$, and H_2O_2 (analytical grade) as a supporting electrolyte. The electrochemical growth of metal oxides is well-known.[14,15] In brief, the OH^- ions formed near the surface of the cathode react with the metal ions (Zn^{2+}, Sn^{2+}, and Sn^{4+}) present in the electrolyte and form ZnO, SnO, and SnO_2, and, with certain precisely controlled parameters, even nanostructures could be prepared with good yield and excellent selectivity.

The XRD patterns of the as-synthesized specimens (not shown here) contain a set of peaks which can indexed to Zn, ZnO, SnO, and SnO_2 phases. The diffraction peak corresponding to Zn is due to the fact that Zn foil is used as a substrate. The XRD patterns of the postannealed specimens I, II, and III are shown in Figure 1a where a set of well-defined diffraction peaks, indexed to the wurtzite hexagonal phase of ZnO, is clear (JCPDS File No. 80-0075). Interestingly, the diffraction peaks corresponding to SnO and SnO_2 phases are not observed after annealing the as-synthesized films. It is expected that during annealing the Sn atoms diffuse inside the ZnO lattice and some of the Zn^{2+} sites are replaced by Sn^{4+}, as the ionic radii of Zn^{2+} (0.74 Å) and Sn^{4+} (0.69 Å) are not very dissimilar. The substitutional presence of Sn^{4+} is anticipated to generate nonuniform stress/strain in the ZnO lattice, which can be envisaged as the broadening of the characteristics diffraction peaks. Furthermore, incorporation of Sn ions in the lattice can also affect the density of the native point defects such as vacancies, interstitials, and antisite defects. It is well-known that the dopants and native point defects generally play an important role in determining the electrical and optical properties of materials. This is due to the presence of localized levels/bands in the band gap of the materials. The XRD pattern specially

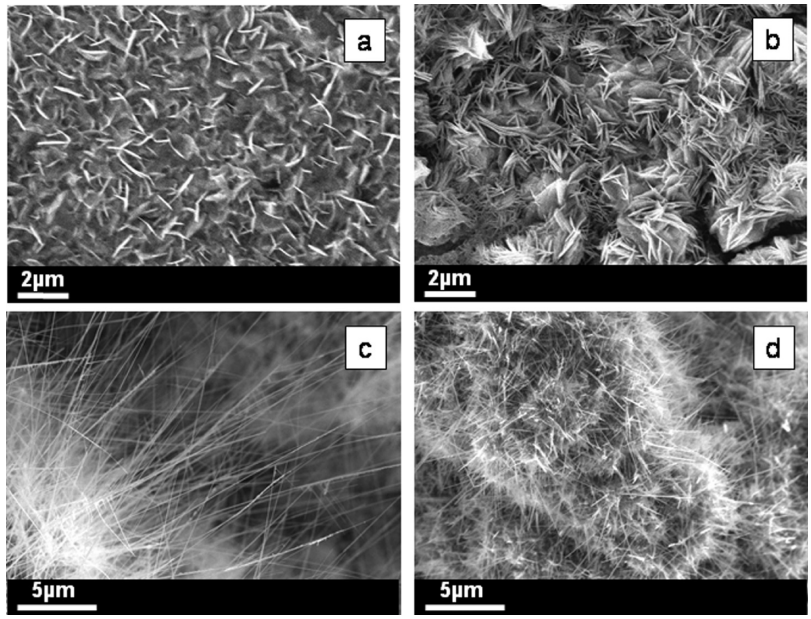

Figure 2. SEM images of specimen I and II (a, b) as-synthesized and (c, d) postannealed in air at 400 °C for 4 h.

acquired using a slow scan rate (Figure 1b) clearly shows a remarkable broadening of the diffraction peaks corresponding to (100), (002), and (101) planes, thereby confirming the substitutional doping of Sn^{4+} at Zn^{2+} sites. The substitutional occupancy of Sn^{4+} ions at the Zn^{2+} sites is also indicated by the XPS analysis, as discussed in the following sections.

The SEM images of as-synthesized and postannealed films are shown in Figure 2. The surface morphology of specimens I and II as seen in Figures 2a and 2b is characterized by a network of densely packed and randomly oriented flakes/sheets despite being mostly perpendicular to the substrate surface. The thickness of these flakes/sheets ranges from 20 to 30 nm and 50 to 200 nm with corresponding diameters between 0.5 and 1 μm and 1 and 2 μm for as-synthesized specimens I and II, respectively. A careful comparison of the SEM images shows that as the deposition time increases, the density of the flakes/sheets becomes higher. The observed surface morphologies can be presumably attributed to a higher growth rate due to the availability of a large number of precursors with the increased deposition time since this constant potential corresponds to growth under diffusion-limited conditions.

It is interesting to note that the surface morphology of the annealed specimens I and II is characterized by the presence of ZnO wires on the entire substrate surface, irrespective of the time of deposition. As seen from Figures 2c−d and 3a−b, the length and average diameter of ZnO wires in specimen I is 20 μm and 88.8 nm, respectively. It is found that the average aspect ratio is ∼225 for 10 min deposition. Similarly, specimen II has wires with the length and the average diameter of 5 μm and 158 nm, respectively, which indicates the average aspect ratio of ∼31. The insets of Figures 3a and b show the size distribution. The ZnO wires are randomly oriented, and a few of them are seen to be protruding outside the substrate surface. A careful observation of the micrographs shows that with the increase in the deposition time the wires become thicker and shorter and exhibit lower areal density. From the EDS spectra, the relative atomic weight percentage of Sn is observed to be 0.5% and 2.0% in the postannealed specimen I and II (not shown here), respectively. Hereafter, the postannealed specimens I and II are referred to as 0.5% and 2% Sn-doped ZnO, respectively.

High resolution XPS scans of Zn-2p, O-1s, and Sn-3d are shown in Figure 4a−c after representing the binding energy

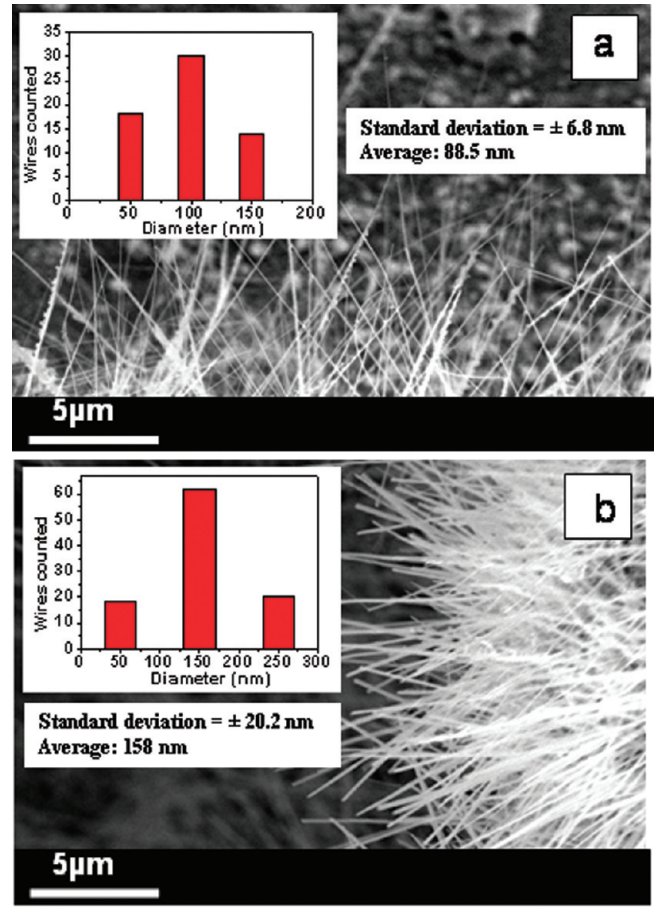

Figure 3. Cross-sectional SEM images of postannealed (a) specimen I and (b) specimen II. The insets show the corresponding diameter distribution of ZnO wires in the specimens.

values with respect to the C-1s peak of carbon at 285 eV as reference. The binding energy of the Zn-$2p_{3/2}$ and Zn-$2p_{1/2}$ peaks located at 1022.5 and 1045.5 eV, respectively, is as shown in Figure 4a. The energy difference between these two peaks is 23 eV, which agrees well with the standard value of 22.97 eV.[28] The scan of the O-1s spectrum is shown in Figure 4b, exhibiting a peak at 531.8 eV which is attributed to oxidized metal ions

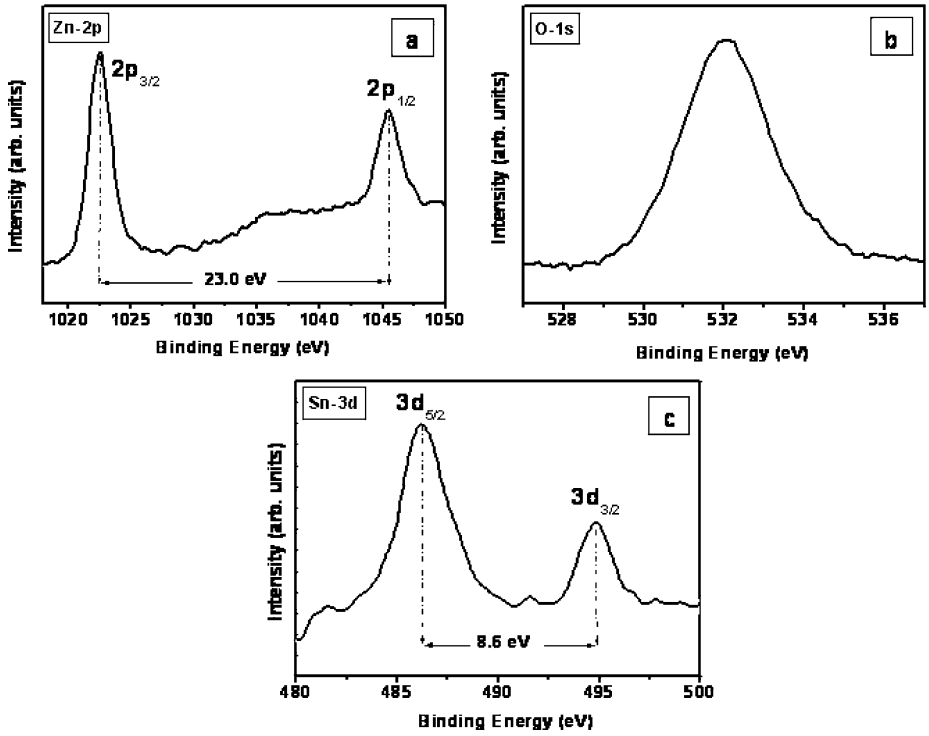

Figure 4. XPS spectra of specimen I (postannealed) (a) Zn spectrum, (b) O spectrum, and (c) Sn spectrum.

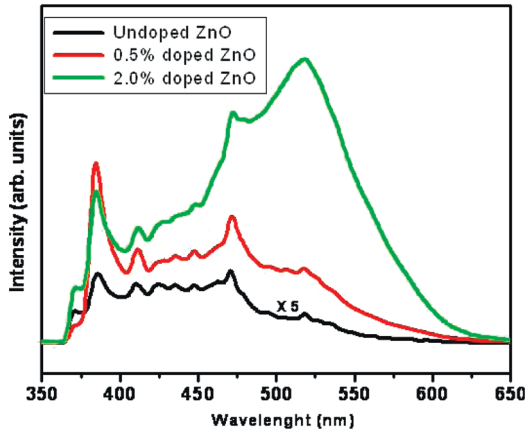

Figure 5. PL spectra of specimen I, II, and III postannealed in air at 400 °C for 4 h.

in the films, viz. O−Sn and O−Zn, in the ZnO lattice. The binding energies of the Sn-3$d_{3/2}$ and Sn-3$d_{5/2}$ as seen in Figure 4c are found to be 486.8 and 495.4 eV, respectively. This indicates that Sn dopant gets incorporated into the films to form O−Sn in the ZnO lattice. Since no characteristic diffraction peaks corresponding to the SnO and SnO_2 are observed in the XRD patterned of postannealed films, the O−Sn bonding can be envisaged by the substitutional doping of Sn ions into the ZnO lattice.

In order to study the effect of Sn concentration on the optical properties of Sn-doped ZnO nanowires, PL spectra were recorded at room temperature and are seen in Figure 5. The ultraviolet (UV) emission band located at ∼384 nm for undoped and doped ZnO nanowires is attributed to near band-edge emission from crystalline ZnO and recombination of free excitons.[29] In addition to this UV emission, the other peaks corresponding to violet, blue, and green (visible) emission bands are seen to be centered at ∼411, ∼435, ∼472, and 518 nm. The blue-green emission is known to originate from the oxygen vacancies and Zn interstitials, produced by the transition of excited optical centers from the deep to the valence level.[30−32] The strong green emission band in the 2% Sn-doped ZnO (postannealed) can be attributed to the high level of structural defects (oxygen vacancies and zinc interstitials and/or presence of Sn ions replaced with Zn ions) in the ZnO lattice structure, which manifest as deep energy levels in the band gap.[20] Thus the intensity of undoped and doped PL spectra corroborates the enhanced defect levels in the specimens, with a corresponding increase in the concentration of Sn.

The field emission current density versus applied field ($J-E$) curves of 0.5% and 2% for Sn-doped ZnO nanowires are shown in Figure 6a. For every specimen, a preconditioning, in terms of removal of any surface asperities and/or contaminants via ion bombardment by keeping the emitter at −2 kV with respect to the anode for 5 min duration, was carried out prior to the $I-V$ measurements. The values of the turn-on field and threshold field, required to draw emission current density of 10 and 100 $\mu A/cm^2$, are observed to be 0.68 and 1.1 V/μm for 0.5% Sn-doped ZnO and 1.72 and 2.25 V/μm for 2.0% Sn-doped ZnO, respectively. These values of the turn-on and threshold field are found to be reproducible and are lower than that of ZnO nanowires (1.91 V/μm),[23] nanoneedles (2.4 V/μm),[25] nanopins (1.92 V/μm),[26] and nanowalls (3.6 V/μm).[27] As the applied voltage increases, the emission current increases rapidly and a current density of ∼750 and 450 $\mu A/cm^2$ could be drawn from the specimens I and II (postannealed) at the applied field of ∼2.45 and 3.15 V/μm, respectively. Interestingly, the turn-on field is found to be influenced by the concentration of Sn in the ZnO thin films, and the lower value has been observed for 0.5% Sn-doped ZnO nanowires. The higher turn-on field for 2% Sn-doped ZnO nanowires can be attributed to lower aspect ratio and/or higher density of point defects in the ZnO nanowires, as seen from the SEM and the PL results.

The emission current density versus applied field characteristic was analyzed by the Fowler−Nordheim (F−N) equation.[33] Figure 6b shows the corresponding $\ln(J/E^2)$ versus $(1/E)$ curve, the F−N plot, derived from the observed $J-E$ characteristics.

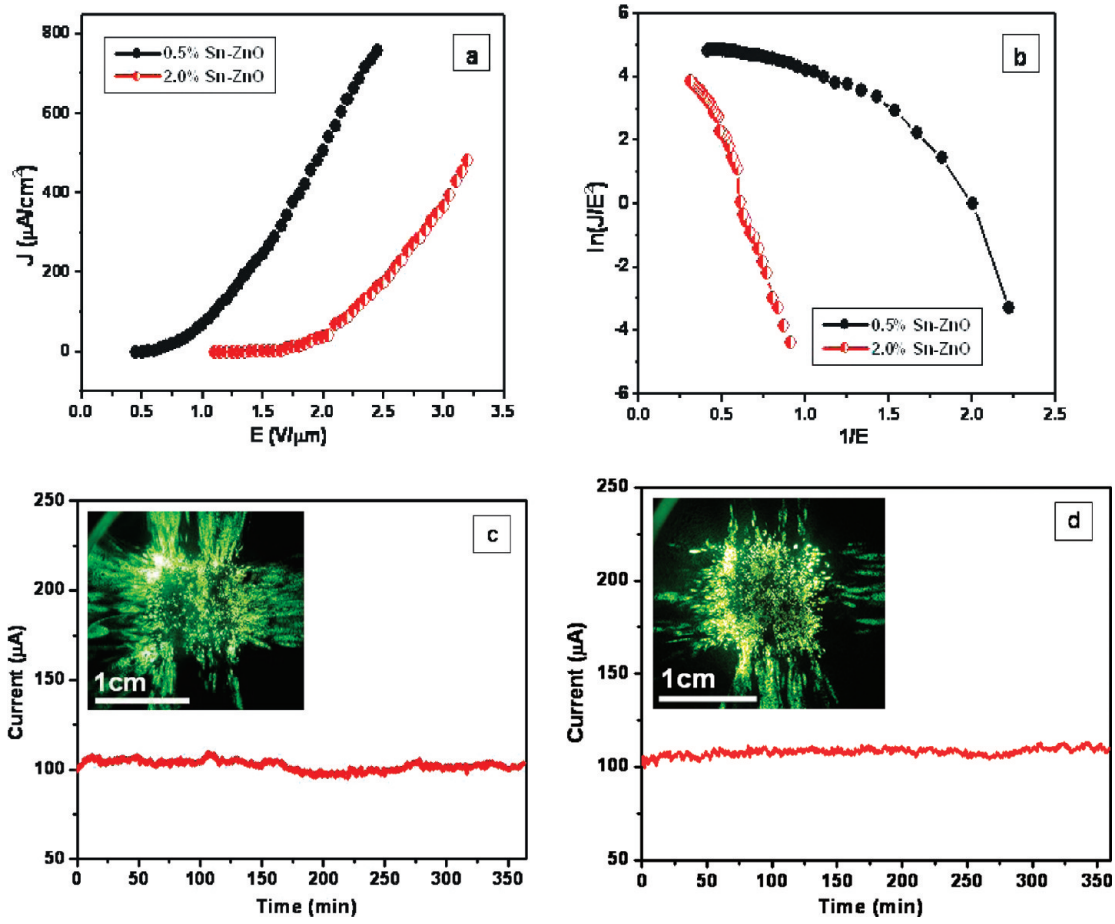

Figure 6. (a) Field emission current density versus applied field ($J-E$) of specimen I and II (postannealed) and (b) corresponding Fowler−Nordheim (F−N) plots, respectively. (c) and (d) Field emission current stability ($I-t$) plots of the specimen I and II (postannealed) without illumination of the visible light, respectively. The insets show the typical field emission images.

The F−N plot exhibits nonlinear behavior over the entire range of the applied field, indicating the semiconducting nature of the emitter. Similar nonlinear F−N plots have been reported for ZnO and other semiconductors.[23,34,35] The nonlinearity exhibited in the F−N plot has been attributed to the semiconducting nature of the emitter material. For semiconducting emitters, the observed nonlinearity can be understood on the basis of the band structure. It is believed that initially, when the applied field is low, the emitted electrons originate mainly from the conduction band states, and as the applied field is increased, the valence band electrons also tunnel out and contribute to the emission current.[34]

The field emission current stability of the 0.5% and 2% Sn-doped ZnO nanowires have been further investigated at a base pressure of $\sim 1 \times 10^{-8}$ mbar. The current versus time ($I-t$) plot for the 0.5% Sn-doped ZnO nanowire emitter required over a duration of 6 h is shown in Figure 6c. The emitter exhibits excellent emission current stability at 100 μA, and the current fluctuations are observed to be within $\pm 5\%$ of the average value. The field emission image captured at the onset of the current stability measurement is shown as inset of the Figure 6c. Similarly, the field emission current stability and field emission image of the 2% Sn-doped ZnO nanowires are shown in Figure 6d. All the observed emission images exhibit a large number of "bright spots", each corresponding to an emission site. This emission image is consistent with the emitter surface morphology. We have also studied the post field emission surface morphology of the emitters where the corresponding SEM images (not indicated here) show no severe deterioration of the emitter surface indicating the robust nature of our ZnO nanowires.

In order to explore the photoinduced field emission behavior of the Sn-doped ZnO nanowire emitter, we have performed the field emission measurements by exposing the cathode to a constant intensity of incident light. Accordingly, plots of photoenhanced field emission current−time curves of 0.5% Sn-doped ZnO specimen, illuminated for different time intervals, are shown in Figure 7. Significantly, we observe a pronounced optical switching effect at different time intervals (Figure 7a), and for longer exposure of light (5 min), the emission current slowly increased to higher values (Figure 7b) while it slowly decreases to the original set value after switching off the lamp (Figure 7c). The increase in the emission current upon light exposure can be attributed to the photogeneration of charge carriers (electron−hole pairs). The maximum rise in the emission current level is seen to be $\sim$100% of the initial value, for the case of long exposure (Figure 7c). The photoenhancement in the field emission current is observed to be reproducible, and the current gets back to the original level after switching the light off. The effect is attributed to the electron−hole recombination process which is consistent with the fact that the photoconductivity decay time (from Figure 7c) is about 65 min. Such a long photoconductivity decay time has been reported for undoped ZnO.[36] To confirm this conjecture, we carried out a simple experiment with the standard photoconductivity measurement setup using a flash lamp (1000 W). A dc voltage

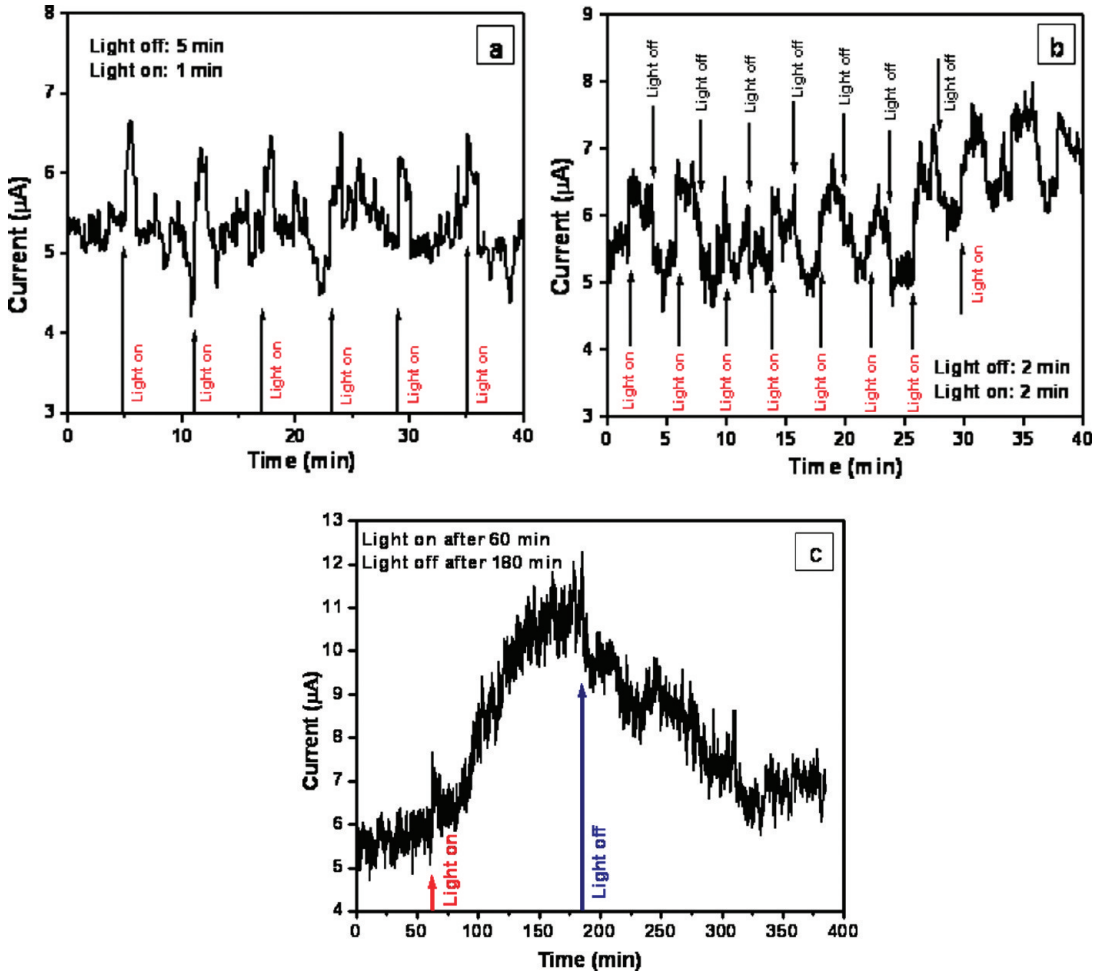

Figure 7. Field emission current stability ($I-t$) plots of specimen I (postannealed) under illumination of the visible light for different durations of time.

of 2−20 V was applied across specimen I. Before the specimen was exposed to the light, it was kept in the dark for the dark current measurement. After it was exposed to the visible light, the current increased 20 times that of the dark current. Hence, the photoenhancement in the field emission current from the Sn-doped ZnO nanowires is attributed to the increased photoconductivity of the specimen. Moazzami et al. have investigated the transient photoconductivity in ZnO epitaxial film under visible excitation.[36] The long photoconductive decay observed in their experiment has been related to the capture of holes in deep trap levels and subsequent hole emission and electron hole recombination. The electron hole pairs are generated upon visible excitation. These excitations correspond to optical transitions between the defect states and the band edge. The PL spectrum (Figure 5) conforms to such optical transition between the defect states. The observed photoenhanced field emission behavior of Sn-doped ZnO nanowires is attributed primarily to the increased photoconductivity. Thus, these results lead not only to the futuristic development of high current density electron sources but also to open up a new area of photoconductivity of Sn-doped ZnO for possible applications in optoelectronic devices and solar cells. Further, there is also possibility of using the photoenhanced field emission behavior as an optical switch in many field emission based devices.

Conclusions

In summary, Sn-doped ZnO nanowire films have been successfully synthesized by potentiostatic electrodeposition on zinc foil. The XRD and XPS analysis shows that the Sn atoms occupy the substitutional zinc site in the wurtzite phase of ZnO. The nanowires with 0.5% Sn doping show a higher aspect ratio than with the 2% Sn-doped nanowires. The 0.5% Sn-doped ZnO nanowires exhibit excellent field emission behavior with the turn-on field 0.68 V/μm for drawing emission current density of 10 μA/cm^2, which is lower than several other nanovariants of ZnO. A current density of 750 μA/cm^2 could be drawn at the field of 2.45 V/μm. A prominent photoenhanced field emission current upon visible illumination of the 0.5% Sn-doped ZnO nanowires films has been observed. The PL and the photoconductivity study of these nanowires show that the observed photoenhanced field emission is due to generation of an electron hole pair from midgap defects states of ZnO. The superior field emission behavior combined with the photoconductivity upon visible light illumination make the 0.5% Sn-doped ZnO nanowires film a promising candidate for the field emission based devices and solar cell applications.

Acknowledgment. F.J.S. thanks Islamic Azad University, Ahwaz Branch, Iran, for the award of a Research Fellowship. The field emission work is carried out as a part of the CNQS, UoP, activity.

Supporting Information Available: Photograph of all metal UHV field emission microscope (FEM) system; movie of the field emission image recorded during the emission current stability measurement at the preset value of 100 μA at the base

pressure of 1×10^{-8} mbar. This material is available free of charge via the Internet at http://pubs.acs.org.

References and Notes

(1) Özgür, Ü.; Alivov, Y. I.; Liu, C.; Teke, A.; Reshchikov, M. A.; Doğan, S.; Avrutin, V.; Cho, S.-J.; Morkoç, H. *J. Appl. Phys.* **2005**, *98*, 041301.

(2) Hu, Z.; Escamilla Ramírez, D. J.; Heredia Cervera, B. E.; Oskam, G.; Searson, P. C. *J. Phys. Chem. B* **2005**, *109*, 11209.

(3) Huang, M. H.; Wu, Y.; Feick, H.; Tran, N.; Weber, E.; Yang, P. *Adv. Mater.* **2001**, *13*, 113.

(4) Yu, H.; Zhang, Z.; Han, M.; Hao, X.; Zhu, F. *J. Am. Chem. Soc.* **2005**, *127*, 2378.

(5) Ramgir, N. S.; Late, D. J.; Bhise, A. B.; Mulla, I. S.; More, M. A.; Joag, D. S.; Pillai, V. K. *Nanotechnology* **2006**, *17*, 2730.

(6) Pan, Z. W.; Dai, Z. R.; Wang, Z. L. *Science* **2001**, *291*, 1947.

(7) Kong, X. Y.; Ding, Y.; Yang, R. S.; Wang, Z. L. *Science* **2004**, *303*, 1348.

(8) Kong, X. Y.; Wang, Z. L. *Nano Lett.* **2003**, *3*, 1625.

(9) Wang, Z. L.; Kong, X. Y.; Zuo, J. M. *Phys. Rev. Lett.* **2003**, *91*, 185502.

(10) Xiang, B.; Wang, P.; Zhang, X.; Dayeh, S. A.; Aplin, D. P. R.; Soci, C.; Yu, D.; Wang, D. *Nano Lett.* **2007**, *7*, 323.

(11) Ryu, Y. R.; Zhu, S.; Han, S. W.; White, H. W.; Miceli, P. F.; Chandrasekhar, H. R. *Appl. Surf. Sci.* **1998**, *127*, 496.

(12) Wu, J.-J.; Liu, S.-C. *J. Phys. Chem. B* **2002**, *106*, 9546.

(13) Heo, Y. W.; Varadarajan, V.; Kaufman, M.; Kim, K.; Nortona, D. P.; Ren, F.; Fleming, P. H. *Appl. Phys. Lett.* **2002**, *81*, 3046.

(14) Peulon, S.; Lincot, D. *Adv. Mater.* **1996**, *8*, 166.

(15) Jamali Sheini, F.; Mulla, I. S.; Joag, D. S.; More, M. A. *Thin Solid Films* **2009**, *517*, 6605.

(16) Mitrushchenkov, A.; Linguerri, R.; Chambaud, G. *J. Phys. Chem. C* **2009**, *113*, 6883.

(17) Kim, K.-K.; Niki, S.; Oh, J.-Y.; Song, J.-O.; Seong, T.-Y.; Park, S.-J.; Fujita, S.; Kim, S.-W. *J. Appl. Phys.* **2005**, *97*, 066103.

(18) Yan, M.; Zhang, H. T.; Widjaja, E. J.; Chang, R. P. H. *J. Appl. Phys.* **2003**, *94*, 5240.

(19) Jie, J.; Wang, G.; Han, X.; Yu, Q.; Liao, Y.; Li, G.; Hou, J. G. *Chem. Phys. Lett.* **2004**, *387*, 466.

(20) Chen, H.; Qi, J.; Huang, Y.; Liao, Q.; Zhang, Y. *Acta Phys.—Chim. Sin.* **2007**, *23* (1), 55.

(21) Li, S. Y.; Lin, P.; Lee, C. Y.; Tseng, T. Y.; Huang, C. J. *J. Phys. D: Appl. Phys.* **2004**, *37*, 2274.

(22) Gulino, A.; Fragala, I. *Chem. Mater.* **2002**, *14*, 116.

(23) Jamali Sheini, F.; Joag, D. S.; More, M. A. *Ultramicroscopy* **2009**, *109*, 418.

(24) Bhise, A. B.; Late, D. J.; Walke, P.; More, M. A.; Mulla, I. S.; Pillai, V. K.; Joag, D. S. *J. Phys. D: Appl. Phys.* **2007**, *40*, 3644.

(25) Marathe, S. K.; Koinkar, P. M.; Ashtaputre, S. S.; More, M. A.; Gosavi, S. W.; Joag, D. S.; Kulkarni, S. K. *Nanotechnology* **2006**, *17*, 1932.

(26) Xu, C. X.; Sun, X. W. *Appl. Phys. Lett.* **2003**, *83*, 3806.

(27) Pradhan, D.; Kumar, M.; Ando, Y.; Leung, K. T. *Nanotechnology* **2008**, *19*, 35603.

(28) In *Handbook of X-ray Photoelectron Spectroscopy*; Muilenbenger, G. E., Ed.; Perkin-Elmer Corporation: Eden Prarie, MN, 1979.

(29) Kong, Y. C.; Yu, D. P.; Zhang, B.; Fang, W.; Feng, S. Q. *Appl. Phys. Lett.* **2001**, *78*, 407.

(30) Vanheusden, K.; Warren, W. L.; Seager, C. H.; Tallant, D. R.; Voigt, J. A.; Gnade, B. E. *J. Appl. Phys.* **1996**, *79*, 7983.

(31) Wang, Y. G.; Lau, S. P.; Lee, H. W.; Yu, S. F.; Tay, B. K.; Zhang, X. H.; Hng, H. H. *J. Appl. Phys.* **2003**, *94*, 354.

(32) Lin, B.; Fu, Z.; Jia, Y. *Appl. Phys. Lett.* **2001**, *79*, 943.

(33) Fowler, R. H.; Nordheim, L. W. *Proc. R. Soc. London, Ser. A* **1928**, *119*, 173.

(34) Ramgir, N. S.; Mulla, I. S.; Vijaymohanan, K.; Late, D. J.; Bhise, A. B.; More, M. A.; Joag, D. S. *Appl. Phys. Lett.* **2006**, *88*, 42107.

(35) Al-Tabbakh, A. A.; More, M. A.; Joag, D. S.; Ramgir, N. S.; Mulla, I. S.; Pillai, V. K. *Appl. Phys. Lett.* **2007**, *90*, 162102.

(36) Moazzami, K.; Murphy, T. E.; Phillips, J. D.; Cheung, M. C.-K.; Cartwright, A. N. *Semicond. Sci. Technol.* **2006**, *21*, 717.

JP911080F